Conformational Behavior of Pyrazine-Bridged and Mixed-Bridged Cavitands: A General Model for Solvent Effects on Thermal "Vase–Kite" Switching

Pamela Roncucci,[a] Laura Pirondini,[a] Giuseppe Paderni,[a] Chiara Massera,[c] Enrico Dalcanale,*[a] Vladimir A. Azov,[d] and François Diederich*[b]

Abstract: The controllable switching of suitably bridged resorcin[4]arene cavitands between a "vase" conformation, with a cavity capable of guest inclusion, and a "kite" conformation, featuring an extended flattened surface, provides the basis for ongoing developments of dynamic molecular receptors, sensors, and molecular machines. This paper describes the synthesis, X-ray crystallographic characterization, and NMR analysis of the "vase–kite" switching behavior of a fully pyrazine-bridged cavitand and five other mixed-bridged quinoxaline-bridged cavitands with one methylene, phosphonate, or phosphate bridge. The pyrazine-bridged resorcin[4]arene cavitand displayed an unexpectedly high preference for the kite conformation in nonpolar solvents, relative to the quinoxaline-bridged analogue. This observation led to extensive solvent-dependent switching studies that provide a detailed picture of how solvent affects the thermal vase–kite equilibration. As for any thermodynamic process in the liquid phase, the conformational equilibrium is affected by how the solvent stabilizes the two individual states. Suitably sized solvents (benzene and derivatives) solvate the cavity of the vase form and reduce the propensity for the vase-to-kite transition. Correspondingly, the kite geometry becomes preferred in bulky solvents such as mesitylene, incapable of penetrating the vase cavity. As proposed earlier by Cram, the kite form is preferred at low temperatures due to the more favorable enthalpy of solvation of the enlarged surface. Furthermore, the kite conformation is more preferred in solvents with substantial hydrogen-bonding acidity: weak hydrogen-bonding interactions between the mildly basic quinoxaline and pyrazine nitrogen atoms and solvent molecules are more efficient in the open kite than in the closed vase form. Vase-to-kite conversion is entirely absent in dipolar aprotic solvents lacking any H-bonding acidity. Thermal vase–kite switching requires fully quinoxaline- or pyrazine-bridged cavitands, whereas pH-controlled switching is also applicable to systems incorporating only two or three such bridges.

Introduction

Among the most fascinating classes of receptors for chemical molecular recognition studies are the resorcin[4]arene cavitands, initially introduced and studied by Cram and co-workers in the early 1980's[1] (Figure 1, top). The "vase"-shaped architecture of the parent quinoxaline-bridged cavi-

[a] P. Roncucci, Dr. L. Pirondini, G. Paderni, Prof. Dr. E. Dalcanale
Dipartimento di Chimica Organica ed Industriale and
Unità INSTM, Università di Parma
Parco Area delle Scienze 17A, 43100 Parma (Italy)
Fax: (+39) 0521-905-472
E-mail: enrico.dalcanale@unipr.it

[b] Prof. Dr. F. Diederich
Laboratorium für Organische Chemie
ETH Zürich, Hönggerberg, HCI, 8093 Zürich (Switzerland)
Fax: (+41) 1-632-1109
E-mail: diederich@org.chem.ethz.ch

[c] Dr. C. Massera
Dipartimento di Chimica Generale ed Inorganica
Chimica Analitica, Chimica Fisica, Università di Parma
Parco Area delle Scienze 17A, 43100 Parma (Italy)

[d] Dr. V. A. Azov
Institut für Organische Chemie
Universität Bremen, Leobener Strasse
NW 2C, 28334 Bremen (Germany)

⌨ Supporting information for this article is available on the WWW under http://www.chemeurj.org/ or from the author.
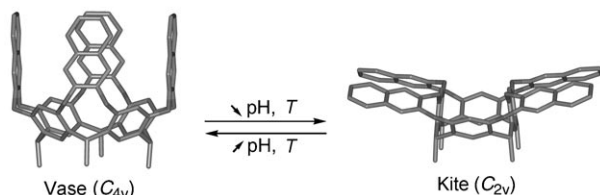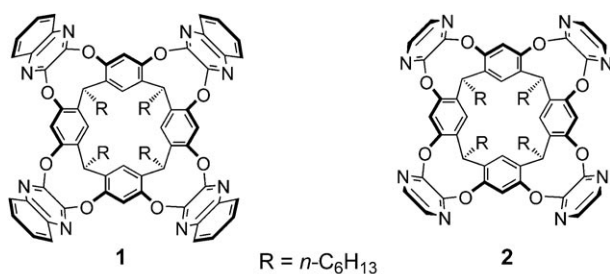
Figure 1. Top: Structures of quinoxaline-bridged (**1**) and pyrazine-bridged (**2**) resorcin[4]arene cavitands. Bottom: Molecular models of the vase and kite conformers of **1**. The equilibrium is temperature- and pH-dependent. Hydrogen atoms and "legs" are omitted for clarity.

tand **1** features a hollow hydrophobic space of about 720 Å^3, suitable for guest complexation.[2,3]

A particularly interesting property of these systems is the reversible switching between a closed "vase" conformation (C_{4v} symmetry), with a deep cavity for guest complexation, and an open "kite" conformation (C_{2v} symmetry) with a flat, extended surface about 19.3 × 15.6 Å in size (Figure 1, bottom), calculated from an available crystal structure.[4] Conformational switching can be reversibly induced by temperature[1] or pH[5] changes, with the kite conformation being preferred at low temperatures and low pH values, or by metal-ion addition.[6] The controllable switching of quinoxaline-bridged cavitands resembles the movement of a mechanical gripper and implies the synthesis of specifically tuned dynamic molecular receptors, sensors, and molecular machines[7] that feature an addressable, geometrically defined switching between the closed vase and opened kite conformations. Significant efforts of our groups were aimed at preparing new modified cavitand architectures[8] and at a detailed exploration of their switching properties, in particular the dependency of the conformational interconversion on environmental factors such as polarity, polarizability, and size of solvent molecules.[5,6b,9] Still, after years of study, very surprising results, not rationalizable within the existing theory, can be encountered.

In this paper, we describe the synthesis and X-ray crystallographic characterization of the pyrazine-bridged cavitand **2**, which, according to NMR switching studies, quite unexpectedly displays high preference for the kite conformation. Besides, five other mixed-bridged quinoxaline-bridged cavitands with a methylene (**3**), phosphonate (**4** and **5**), or phosphate (**6** and **7**) bridge were synthesized to explore the effect of different bridging groups on the vase–kite equilibrium. A general model of solvent effects on vase–kite isomerization is presented.

Results and Discussion

Synthesis and X-ray crystal structure of pyrazine-bridged cavitand 2: The synthesis of pyrazine-bridged cavitand **2** was carried out following the established procedure for the preparation of homo-bridged cavitands.[1] Specifically, resorcin[4]arene **8** was treated with 2,3-dibromopyrazine in the presence of K$_2$CO$_3$ to give **2** in 50% yield (Scheme 1).
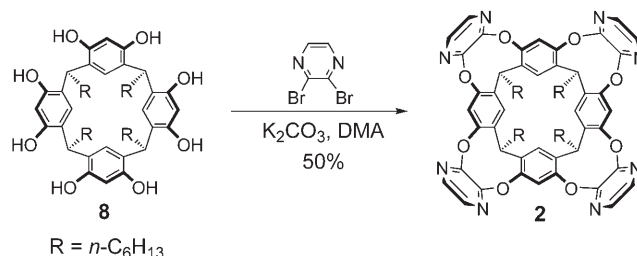
Scheme 1. Synthesis of pyrazine-bridged cavitand **2**. DMA = N,N-dimethylacetamide.

Crystals of **2** were obtained by exposing a solution of the compound in dichloromethane to ethanol vapors. The X-ray crystal structure analysis shows the cavitand in the vase conformation (Figure 2, the atomic numbering scheme is dis-
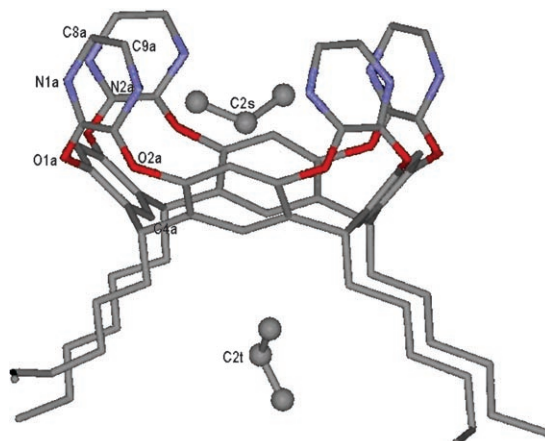

Figure 2. Perspective view of **2** showing the two disordered ethanol molecules, one inside the intramolecular cavity and the other in the void between the alkyl chains. The hydrogen atoms are omitted for clarity.

played for subunit **a** and identically repeated in the remaining three subunits). Partially disordered solvent is localized within the cavity and in the crystal lattice (three ethanol molecules for each cavitand molecule). One ethanol molecule is hosted in the large intramolecular void available at the end of the aliphatic chains attached to the bridging carbon atoms of the macroring, the atom C2t being 3.35(1) Å below the reference mean-square plane R passing through C4a, C4b, C4c, C4d. The second ethanol molecule is located in the intramolecular cavity with the atom C2s 2.45(1) Å above the reference plane R. The third ethanol

molecule fills the intermolecular voids of the crystal lattice. In all three cases, large intermolecular host–guest distances are indicative of only weak attraction between the cavitand and the solvent molecules. In the crystal lattice, the molecules of **2** display a head-to-head arrangement with a small shift between the pseudocavity axes, in contrast to the known X-ray structures[3a,b,5a,8c] of quinoxaline-bridged cavitand **1** featuring infinite head-to-tail columns.

The large intramolecular cavity of the cavitand available for complexation can be described as a truncated cone surmounted by a cylinder (Figure 3). The principal dimensions
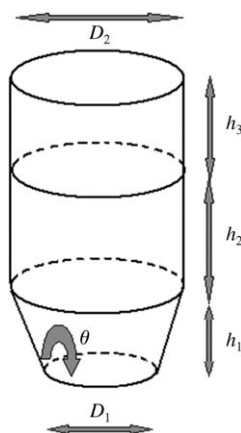

Figure 3. Schematic representation of the cavitand architecture. h_1: height of the truncated cone formed by the atoms C4a–d on the bottom and O1a–d/O2a–d on the top; θ: opening angle of the cone; h_2: height of the bottom cylinder formed by the atoms O1a–d/O2a–d on the bottom and C8a–d/C9a–d on the top; h_3: height of the upper cylinder added by extra benzene ring of quinoxaline (related to quinoxaline-bridged cavitands only); D_1: minor diameter formed by the atoms C4a–d on the bottom of the cavity; D_2: average diameter measured at the mouth of the cavity. Labeling of the atoms refers to cavitand **2**, Figure 2.

of cavitand **2** are given in Table 1 along with those obtained from the X-ray crystal structure of **1**[3a,b] for comparison. The cylinder, bound on the top by the circular ribbon of the atoms C8 and C9 of the pyrazine and on the bottom by the bridging O1 and O2 atoms, has a diameter D_2 of 8.989(5) Å, measured at the mouth of the cavity, and a height h_2 of 2.904(6) Å. The truncated cone, bound on the top by the cir-

Table 1. Geometrical dimensions for cavitands **1** and **2**, and resorcinarenes **3** and **4**. Values are calculated from averaged interatomic distances.[a]

	1	**2**	**3**	**4**
D_1 [Å]	5.013(6)	5.173(5)	5.227(4)	5.238(7)
D_2 [Å]	8.013(5)	8.989(5)	–	–
θ [°]	125.5(2)	133.8(1)	124.4(1)	125.2(1)
θ_1 [°]	83.6(2)	83.47(7)	84.68(3)	84.5(2)
h_1 [Å]	2.209(4)	1.734(3)	2.248(3)	2.28(4)
h_2 [Å]	3.420(5)	2.904(6)	3.352(4)	3.45(3)
h_3 [Å]	2.365(5)	–	2.385(5)	2.38(2)

[a] For the definition of most parameters, see Figure 3. θ_1 is defined as the average angle between the mean-square plane passing through the bridging oxygen atoms and the four pyrazine planes.

cular array of the atoms O1 and O2 (shared with the cylinder) and on the bottom by the atoms C4a–d, has a minor diameter D_1 of 5.173(5) Å and a height h_1 of 1.734(3) Å. It can be emphasized that cavitand **2** is significantly different from **1** in the common parameters (D_1, D_2, h_1, h_2, θ): the cylinder in **2** is almost 0.5 Å shorter (h_2) and about 1.0 Å larger (D_2) than in **1** and the cone is more open ($\theta = 133.8(1)$ vs. 125.5(2)°). In contrast, the dihedral angle θ_1 (defined as the average angle between the mean-square plane passing through the bridging oxygen atoms and each of the four pyrazine planes) is quite similar to that of **1** ($\theta_1 = 83.47(7)$ vs. 83.6(2)°). Overall, the cavity of pyrazine-bridged cavitand **2** is 3.4 Å shallower than that of quinoxaline-bridged **1** (Table 1).

Synthesis and X-ray crystal structures of mixed-bridged cavitands: Trisquinoxaline-bridged cavitand **9** was prepared by reacting resorcin[4]arene **10** with three equivalents of 2,3-dichloroquinoxaline. The methylene-bridged target compound **3** was subsequently obtained by bridging **9** with CH_2BrCl in Me_2SO (Scheme 2).

Phosphonate-bridged cavitands **4** and **5** were prepared by reacting phenylphosphonic dichloride with trisquinoxaline-bridged cavitand **9** and Et_3N in dry THF, whereas acetone was used as the solvent for the reaction between cavitand **9** and *p*-tolyl dichlorophosphate to yield the phosphate-bridged cavitands **6** and **7** (Scheme 2). The presence of a stereogenic phosphorus(v) center gives rise to two diastereomers in which the P=O group is oriented either inward (in) or outward (out) with respect to the cavity. The configuration of all diastereomers was assigned by established spectroscopic methods[10] and confirmed in the case of **4** by X-ray structure analysis. Particularly diagnostic is the upfield shift of the aromatic protons of the phenyl substituents on the phosphorus atom upon inclusion within the cavity (out isomers).

Crystals of methylene-bridged **3** were obtained from a solution of dichloromethane and ethyl acetate. Similar to **1** and **2**, cavitand **3** also prefers the vase conformation in the solid state (Figure 4, top) with the formation of head-to-head dimers (Figure 4, bottom). Two ethyl acetate molecules for each independent unit were found in the solid state. One, statistically distributed over two different orientations, is located inside the cavity of the receptor with the C4r atom lying 2.77(1) Å from the least-squares plane passing through C1a, C1c, C1d, and C1e; the second is positioned in the intermolecular holes of the crystal lattice, stabilized by van der Waals interactions with the nearest neighboring molecules. The values of D_1, h_1, h_2, h_3, θ, and θ_1 (Figure 3) for **3** are reported in Table 1.

Crystals of phosphonate-bridged cavitand **4** were obtained by slow evaporation of a solution of the sample in dichloromethane. The crystal structure of **4** is shown in Figure 5 (top). It crystallizes with a disordered water molecule, which is presumably taken from the environment, inside the intramolecular cavity. Other water molecules and a dichloromethane molecule are found in the voids of the crystal lattice.
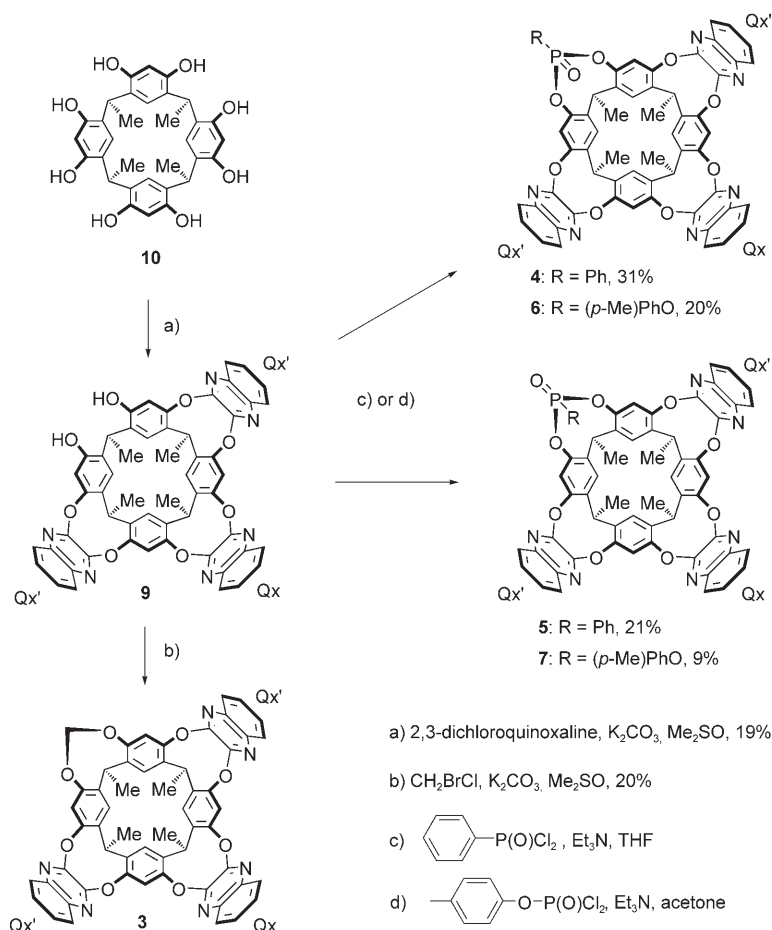
Scheme 2. Synthesis of methylene-bridged cavitand **3**, phosphonate-bridged cavitands **4** ("in") and **5** ("out"), and phosphate-bridged cavitands **6** ("in") and **7** ("out").

In the crystal packing, the cavitands form dimeric structures, with the phenyl ring of the phosphonate group pointing inside the free cavity of the opposite cavitand (Figure 5, bottom). Thus in the solid state, the cavities prefer the inclusion of aromatic guests with respect to crystallization solvents.

The rather poor data and the limited number of reflections prevented an accurate discussion on the bond lengths and angles, but it nevertheless allowed establishing the shape and the main geometrical parameters of the macrocyclic structure, which prefers the vase conformation in the solid state (Table 1). In both cases (**3** and **4**) the introduction of a different fourth bridge does not modify significantly the vase structure in the solid state.

¹H NMR switching studies of the pyrazine-bridged cavitand 2: As it was shown before,[1,5] cavitand **1** with four quinoxaline bridges experiences a dynamic equilibrium between vase and kite conformations (Figure 1, bottom); the vase form is preferred at $T > 290$ K, whereas the kite conformer is predominant below 230 K. Besides, the equilibrium between the two degenerate kite conformations becomes fast on the NMR timescale above 210 K.[5b] The kite 1–kite 2

equilibration of **1** was studied in acidic solutions, in which the kite conformation is the only existing one throughout the entire temperature range. The vase–kite equilibrium is conveniently monitored by ¹H NMR spectroscopy: in the vase form, the methine protons in the resorcin[4]arene skeleton appear at $\delta \approx 5.5$ ppm, whereas upon switching to the kite form, this resonance shifts upfield to $\delta \approx 3.7$ ppm.

¹H NMR spectra of cavitand **2** in CDCl₃ undoubtedly indicated a dynamic behavior at room temperature (Scheme 3), with broadened lines in the aromatic region and the methine resonance broadly smeared between $\delta = 3.6$ and 5.6 ppm.

Variable-temperature (VT) NMR studies of pyrazine-bridged **2** in CDCl₃ demonstrated that the vase conformation is favored at higher temperatures and that the kite structure is the predominant conformation at lower temperatures as in the case of quinoxoline-bridged **1**. Nevertheless, the vase-to-kite transition occurred at much higher temperatures compared with **1**, which is fixed in the vase conformation at room temperature and starts to display the transition to the kite conformation only 20–30 degrees below. Fully resolved ¹H NMR spectra of the vase conformation of **2** were obtained only at 353 K, whereas the quinoxaline-bridged cavitand spectrum displayed a resolved (vase) spectrum already at 293 K. Low-temperature experiments (below 273 K) demonstrated the disappearance of the vase conformation at approximately 263 K; nevertheless, even below this temperature, the aromatic resonances were broadened down to 223 K due to kite 1–kite 2 equilibration on the NMR timescale (Figure 6). Only at 223 K did the ¹H NMR spectra become fully resolved, showing an AX system for the pyrazine protons and a complex multiplet for the (resorcin[4]arene) methine protons. The absence of the vase conformation below 263 K gave an opportunity to determine for the first time activation parameters for the kite 1–kite 2 equilibration in neutral solution, which was not possible for **1** due to the lower temperature of the vase→kite transition. The parameters for cavitand **2** were found to be: $\Delta H^{\ddagger} = 12.4 \pm 1.5$ kcal mol⁻¹, $\Delta S^{\ddagger} = 0.1 \pm 3$ cal mol⁻¹ K⁻¹ (Table 2).

Titration of **2** in CDCl₃ with trifluoroacetic acid (TFA) at 298 K displayed a behavior similar to that of **1**: the methine
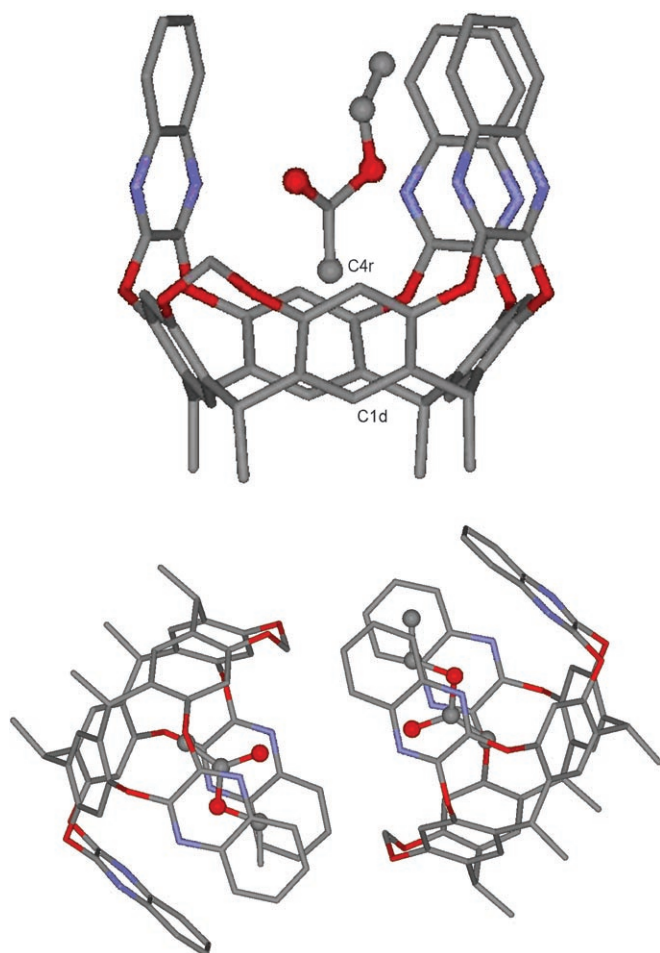
Figure 4. Top: Perspective view of **3** showing the ethyl acetate molecule inside the intramolecular cavity. Bottom: Head-to-head arrangement of **3** in the crystal lattice. Hydrogen atoms are omitted for clarity, only one alternative orientation of the cavity-bound ethyl acetate molecule is shown.

multiplet shifted to about 3.8 ppm (corresponding to the kite conformation) at 0.1 M TFA, and all resonances became fully resolved at ~0.3 M TFA, indicating complete switching of **2** to the kite conformation.

VT-NMR studies of cavitand **2** in acidic solution (0.75 M TFA) in CDCl₃ displayed a fast kite 1–kite 2 equilibrium at higher temperatures that slowed down upon cooling below 273 K, a behavior reminiscent of that of quinoxoline-bridged **1**. NMR modeling was performed with this set of VT spectra in order to determine the activation parameters of the kite 1–kite 2 equilibration of pyrazine-bridged **2** in acidic solution. Quite unexpectedly, they were found to be: $\Delta H^{\ddagger} = 12.6 \pm 1.5$ kcal mol⁻¹, $\Delta S^{\ddagger} = -3.2 \pm 3$ cal mol⁻¹, very similar to the values for neutral chloroform (Table 2). Thus, in both neutral and acidic media, the kite 1–kite 2 switching is likely to proceed through similar transition states. Activation entropy and enthalpy differ sharply from those measured for the cavitand **1** kite 1–kite 2 switching mode in acidic solution[5b] (Table 2). The kite 1–kite 2 switching process presumably involves a vase-type transition state,[5b] which requires a
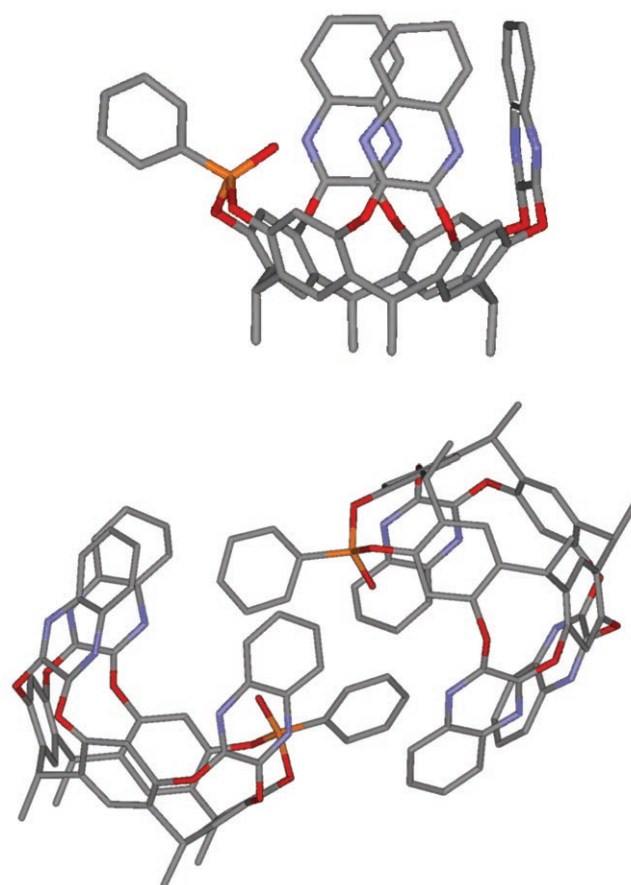
Figure 5. Top: Perspective view of **4**. Bottom: Head-to-head arrangement of **4** in the crystal lattice. Hydrogen atoms and the disordered water molecule inside the cavity are omitted for clarity.
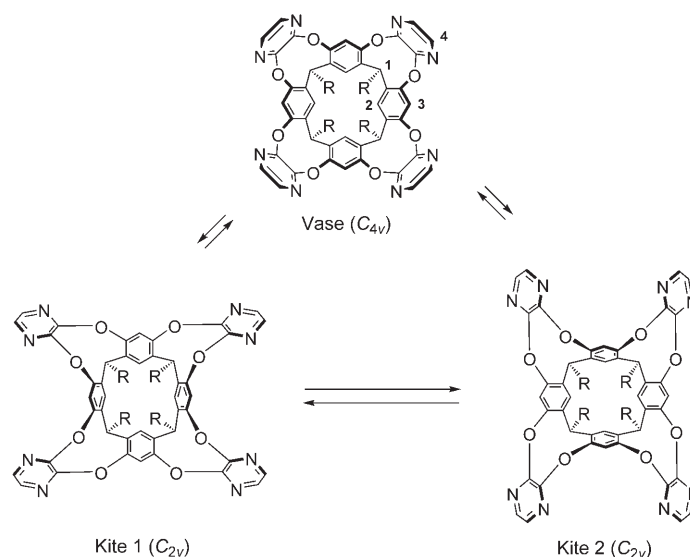
Scheme 3. Interconversions between vase, kite 1, and kite 2 conformations of the resorcin[4]arene cavitand with four pyrazine flaps.

large degree of desolvation. Hence the activation enthalpy, due to loss of solvation, is much more unfavorable in the case of **1** with its larger surface, while at the same time
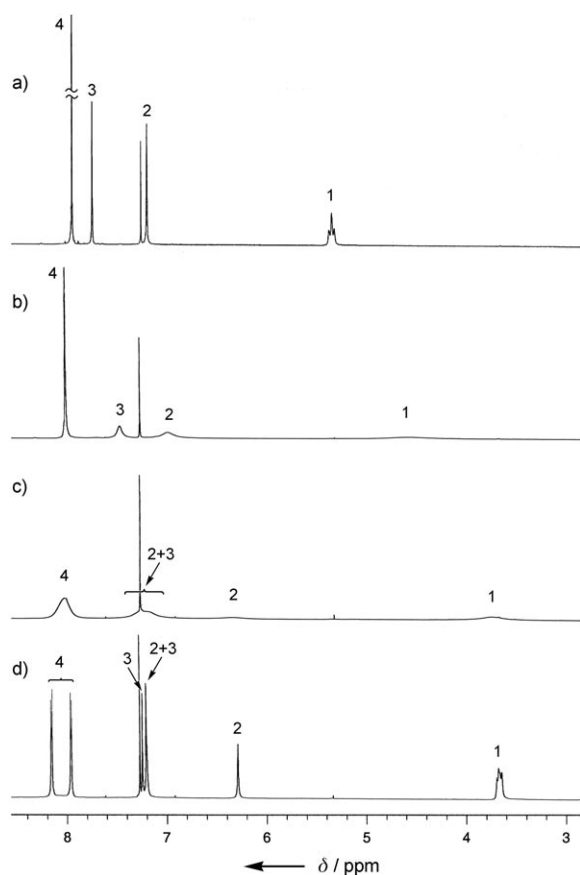
Figure 6. ^{1}H NMR spectra of **2** ($c = 1 \times 10^{-2}$ M, 300 MHz, CDCl$_3$) at different temperatures: a) $T = 353$ K (cavitand frozen in the vase conformation); b) $T = 283$ K (equilibration of the vase and the kite conformations); c) $T = 258$ K (kite 1–kite 2 equilibration on the NMR timescale); d) $T = 223$ K (cavitand frozen in the kite conformation). For peak assignment see Scheme 3. Singlet at 7.26 ppm belongs to CDCl$_3$.

Table 2. Thermodynamic and kinetic parameters for different switching modes of **1** and **2**.

| Cavitand	Conditions	Switching Mode	$\Delta H^{\ne}$ [kcal mol^{-1}]	$\Delta S^{\ne}$ [cal mol^{-1} K^{-1}]
1[a]	CD$_2$Cl$_2$, 0.75 M TFA	kite 1–kite 2	21.2 ± 1.5	26.6 ± 3
2	CDCl$_3$, 0.75 M TFA	kite 1–kite 2	12.6 ± 1.5	-3.2 ± 3
2	CDCl$_3$	kite 1–kite 2	12.4 ± 1.5	0.1 ± 3

[a] Values adopted from reference [5b]. TFA = trifluoroacetic acid.

the desolvation entropy is more favorable than in the case of **2**.

The higher preference for the kite conformation of **2**, compared with **1**, is quite remarkable. According to the commonly accepted theory[1] suggested by Cram in the 1980s, the favorable enthalpy of solvation of the larger kite surface (as compared to the smaller vase surface) is the main driving force for the vase→kite transition of the quinoxaline-bridged cavitands, overriding the slightly higher strain of the four dioxa-containing nine-membered rings in

the kite form. In the case of pyrazine-bridged cavitand **2** (ca. 200 Å^2), the area of the kite surface is much smaller with respect to **1** (ca. 300 A^2);[1,4] nevertheless, it shows a higher relative preference for the kite conformation! This result led us to extend the switching model proposed by Cram by establishing the hypothesis, that not only a higher kite stabilization, but also a weaker vase stabilization are the solvent-mediated driving forces for the vase→kite transition.

Solvent dependence of the vase–kite conformational switching: To better understand the factors influencing the vase–kite equilibrium, we undertook a solvent scan of the conformational behavior of **2** at room temperature. The results are summarized in Table 3.

Table 3. Solvent scan of the vase–kite equilibrium of **2** at 298 K. The $\Sigma\alpha$ and $\Sigma\beta$ values are taken from references [12].

	Solvent	$\Sigma\alpha$	$\Sigma\beta$	Conformation	δ (CHAr$_2$) [ppm]
1	[D$_6$]benzene	0.00	0.14	vase	6.00
2	[D$_8$]toluene	0.00	0.14	vase	5.87
3	[D$_5$]nitrobenzene	0.00	0.28	vase	5.79
4	[D$_4$]1,2-dichlorobenzene	0.00	0.04	vase	5.77
5	[D$_{12}$]mesitylene	0.00	0.19	fluxional	5.63
6	CD$_2$Cl$_2$	0.10	0.05	fluxional	5.06
7	CDCl$_2$CDCl$_2$	0.16	0.12	fluxional	4.78
8	CDCl$_3$	0.15	0.02	fluxional	4.93
9	CDBr$_3$	0.15	0.06	fluxional	4.83
10	CH$_3$CCl$_3$	0.00	0.09	vase	5.85
11	C$_2$Cl$_4$	0.00	0.00	vase	5.45
12	CCl$_4$	0.00	0.00	vase	5.79
13	(CD$_3$)$_2$SO	0.00	0.78	vase	5.48
14	(CD$_3$)$_2$CO	0.04	0.49	vase	5.66
15	CS$_2$	0.00	0.07	vase	5.65
16	[D$_8$]THF	0.00	0.48	vase	5.73
17	[D$_{12}$]cyclohexane	0.00	0.00	vase	5.78
18	pyrazine	0.00	0.62		–
19	quinoxaline	0.00	0.59		–

Two different factors contribute to the destabilizing of the vase conformation in pyrazine-bridged **2**: cavity solvation and solvent hydrogen-bonding acidity. Cavitand **1** has a deep cavity with four polarizable quinoxaline walls that is efficiently stabilized by polarizable chlorinated solvents and, especially well, by the aromatic solvents that are nearly complementary to the cavity size.[11] In contrast, cavitand **2** has a shallower cavity with less polarizable pyrazine walls (Table 1); therefore, stabilization of the cavity by solvation is less efficient in comparison with **1**.

Studies of **2** in [D$_8$]toluene (entry 2) revealed that it is fixed in the vase conformation even at low temperatures (223 K), like a similar derivative with eight chloride substituents on the pyrazine rings.[1b] Nevertheless, **2** switches to the kite conformation upon addition of TFA 0.5 M, displaying a behavior similar to **1**.[5b] Cavitand **2** was also fixed in the vase conformation in benzene, nitrobenzene, and 1,2-dichlorobenzene (entries 1, 3, 4) and, similarly to toluene, could be switched to the kite conformation upon addition of

TFA > 0.5 M. Unfortunately, the conformational behavior of the octachlorinated cavitand[1b] has been studied only in [D$_8$]toluene, therefore a more precise comparison cannot be made.

Unlike the smaller benzene-based solvents, deuterated mesitylene (entry 5) cannot stabilize the vase conformation of **2**. As a result, all the resonances remained broadened at 295 K, displaying resolved peaks corresponding to the vase conformer only at approximately 350 K. Upon cooling to 253 K, the spectrum featured a pattern corresponding to the slow exchange between the vase and kite conformations. Thus, similar to cavitand **1**, the vase conformation of **2** is destabilized, since the bulky mesitylene molecules do not fit inside the cavity. On the other hand, toluene, benzene, nitrobenzene, and 1,2-dichlorobenzene stabilize preferentially the vase conformation as a consequence of a better fitting of these solvents into the inner cavity of the vase structure. In the case of halogenated hydrocarbons, the trend is not unequivocal. Cavitand **2** is either fluxional (entries 6–9) or fixed in the vase form (entries 10–12) at room temperature, depending on the solvent used. This conflicting behavior cannot be rationalized in terms of different van der Waals interactions between the solvent and the vase and kite forms, but it requires the introduction of a second intermolecular interaction mode.

We identified weak solute–solvent hydrogen-bonding interactions as the second interaction mode. A linear solvation energy relationship (LSER) has been reported that describes and quantifies solute–solvent interactions, with the hydrogen-bonding acidity ($\Sigma\alpha$) and basicity ($\Sigma\beta$) being key parameters.[12] The $\Sigma\alpha$ and $\Sigma\beta$ values of all solvents used in the conformation analysis of **2** are reported in Table 3 together with the hydrogen-bond basicity of pyrazine and quinoxaline (entries 18 and 19). According to the reported data, pyrazine nitrogen atoms are slightly more basic than the corresponding quinoxaline ones found in **1**, as expected.

Within the chlorinated hydrocarbon series (entries 6–12), whenever the hydrogen-bonding acidity $\Sigma\alpha$ is substantial, cavitand **2** is fluxional at room temperature. Instead, when $\Sigma\alpha = 0$, cavitand **2** adopts the rigid vase form. It becomes clear that solvent polarizability and van der Waals interactions are not the only factor favoring the switching to the kite geometry. Instead, weak hydrogen-bonding interactions between solvent and the basic nitrogen atoms of the pyrazine (and quinoxaline)-bridged cavitands are important to provide additional stabilization to the kite form. In the open kite geometry, the cavitand nitrogen atoms are much more accessible for undergoing such weak hydrogen-bonding interactions with solvent molecules than in the closed vase geometry, which explains why such interactions shift the equilibrium towards the kite conformation. Furthermore, the slightly higher basicity of the pyrazine nitrogen atoms should also make a contribution to the observed higher tendency of **2** to adopt the kite conformation.

The absence of significant hydrogen-bonding acidity ($\Sigma\alpha \approx 0.00$) presumably is also the reason why **2** (and **1**) prefer the vase form in dipolar aprotic solvents such as Me$_2$SO,

acetone, carbon disulfide, and THF (entries 13–16). Also, in the aromatic solvents series (entries 1–4) the relationship between preferential vase conformation and absence of hydrogen-bonding acidity is respected, even if in this case preferential solvation of the cavity in the vase form is presumably the major player. This is confirmed by the behavior of mesitylene (entry 5), which destabilizes the vase conformer since it is too large to fit within the cavity.

^{1}H NMR switching studies of the mixed-bridged cavitands: Cram's interpretation of the vase–kite equilibrium in quinoxaline-bridged **1**, based on the different solvation of the two conformers, implies the presence of a completely delimited cavity with a single entrance for the vase form. Only in this case, the differential solvation among the two conformers is sizable. To verify this hypothesis, we studied the conformational behavior of mixed-bridged cavitands **3–7**, with one of the four quinoxaline wings displaced by a different bridge, leaving a wider entrance. None of the mixed-bridged cavitands displayed VT-triggered switching in CD$_2$Cl$_2$ and were fixed in the vase conformation over the entire temperature range from 203 to 313 K. Addition of TFA (1 M) led to the shift of the methine protons, neighboring the quinoxaline bridges, from $\delta \sim 5.9$ ppm to ~4.2 and ~4.6 ppm (the resonance of the methine proton near the other bridge remained at about $\delta = 4.9$ ppm) and to the change of the aromatic region pattern, indicating the opening of the quinoxaline flaps. Similar behavior was previously observed for the cavitand **3** with one methylene bridge.[5b] Addition of base (K$_2$CO$_3$) to the acidic solution reversibly led to the initial spectra, indicating the transition to the initial conformation. The inward (**4**, **6**) or outward (**5**, **7**) orientation of the P=O groups[10] in cavitands **4–7** does not influence the stability of the vase conformer.

The thermal vase–kite equilibrium in neutral solutions completely depends on the integrity of the four cavity walls. The absence of a single quinoxaline moiety switches off the thermal vase-to-kite interconversion by substantially decreasing the solvation of the kite form. Mixed-bridged cavitands can only adopt the kite conformation by protonation of the quinoxaline nitrogen atoms with an acid such as TFA, as a result of the developing Coulombic repulsion in the vase geometry.

Conclusions

Based on the present study, a much clearer picture now emerges how solvent affects the thermal vase–kite equilibration of quinoxaline- and pyrazine-bridged cavitands. The earlier proposal by Cram that the kite geometry is preferred at low temperatures due to the larger enthalpy of solvation of the more extended kite surface (as compared to the vase surface) remains fully valid but needs to be extended by several parameters. The correlation of kite stabilization with surface area is demonstrated in an impressive way by the activation parameters for the kite 1–kite 2 interconversion of

quinoxaline-bridged **1** and pyrazine-bridged **2**. The vase-like transition state of this interconversion requires substantial desolvation, and this is clearly reflected in the enthalpy and entropy of activation. The conformational interconversion of **1**, with its much larger surface relative to **2**, is enthalpically less favorable, due to loss of solute–solvent interactions, but at the same time entropically much more favorable as a result of solvent release from the surface. However, an extended solvent scan revealed for the first time that kite stabilization not only results from enhanced solvent–surface van der Waals interactions, but also from weak hydrogen-bonding interactions between the mildly basic pyrazine and quinoxaline nitrogen atoms and solvent molecules with a substantial hydrogen-bonding acidity as measured by $\Sigma\alpha$ values. For steric reasons, such interactions are less effective in the vase form. The kite geometry is also more favorable for the pyrazine- than for the quinoxaline-bridged cavitands, due to the higher hydrogen-bonding basicity of the latter. In fact, vase-to-kite conversion is entirely absent in dipolar aprotic solvents lacking any hydrogen-bonding acidity. Free energy simulations in the liquid state are planned to further support the existence of this hitherto unrecognized solvation mode.

The major addition to the initial rational developed by Cram considers that thermodynamic equilibria, such as conformational isomerisms, are two-state functions and that not only the stabilization of the kite but also of the vase form needs to be taken into account in explaining experimental results. This is nicely revealed by the fact that **2**, despite its smaller surface, has a higher preference for the kite geometry than **1**. The cavity of **1** in the vase form is more extended and deeper than the cavity of **2**. As a result, suitably-sized solvent molecules, such as benzene, toluene, or 1,2-dichlorobenzene solvate and stabilize the deeper vase form of **1** more efficiently than the shallower vase form of **2** (see Figures 2 and 3 and Table 1). This vase stabilization overweighs the kite stabilization and leads to a less favorable vase-to-kite transition in the case of **1**, while the reduced vase stabilization is at the origin of the facilitated transformation into the kite form in the case of **2**. The importance of vase stabilization is seen with both cavitands in a solvent such as mesitylene, which is too bulky to fit into the cavity: due to the lack of inner solvation, the kite geometry becomes much more preferable. Finally, thermal vase–kite switching requires fully quinoxaline- or pyrazine-bridged cavitands, whereas pH-controlled switching is also applicable to systems incorporating only three such bridges.

The described class of cavitands provides fascinating modules for molecular switches[9] and, possibly in the future, for molecular machines. Such developments towards technologies and device fabrication greatly benefit from the understanding of the basic physical–organic principles governing the switching process.

Experimental Section

General: Reagent-grade solvents and reagents were purchased and used without further purification. Resorcin[4]arenes **8** and **10**[13] and 2,3-dibromopyrazine[14] were prepared according to literature procedures. Solvents were dried over 3 and 4 Å molecular sieves. All reactions were carried out under Ar or N_2 atmosphere. ^{1}H NMR spectra were recorded in CDCl$_3$ on Bruker AC300 (300 MHz), Avance (300 MHz), and AMX400 (400 MHz) spectrometers; chemical shifts (δ) are reported in parts per million (ppm) downfield from tetramethylsilane using the residual solvent peak as internal reference. ^{31}P NMR spectra were recorded on a Bruker AMX400 (162 MHz), with the chemical shifts reported in ppm relative to external 85% H_3PO_3 at $\delta = 0.00$ ppm. FT-IR spectra were recorded on a Nicolet 5PC spectrometer. Mass spectra of the organic compounds were measured with a Finnigan MAT SSQ710 spectrometer, using the CI (chemical ionization) technique. Melting points (m.p.) were obtained with an electrothermal capillary melting-point apparatus and were not corrected. Microanalyses were performed by using the facilities at Parma University. Analytical thin-layer chromatography (TLC) was performed on precoated SiO$_2$ glass plates with F-254 fluorescent indicator. Column chromatography was carried out by using silica gel 60 (70–230 mesh) from Merck.

Pyrazine-bridged cavitand 2: A mixture of resorcinarene **8** (0.72 g, 0.87 mmol), K$_2$CO$_3$ (1.21 g, 8.81 mmol), and 2,3-dibromopyrazine (1.04 g, 4.42 mmol) in dry DMF (20 mL) was stirred in a sealed tube at 80 °C for 1 d. The reaction was quenched by the addition of HCl$_{aq}$ (10%), and the solid formed was filtered, washed with water, and dried. The crude product was purified by column chromatography on silica gel by using hexane/EtOAc (8:2 v/v) to give compound **2** as a white solid (0.50 g, 0.44 mmol, 50%). M.p. 142–144 °C; ^{1}H NMR (300 MHz, CDCl$_3$): $\delta = 0.87$ (t, $^{3}J = 6.4$ Hz, 12H; CH_3), 1.28 (m, 32H; $(CH_2)_4$), 2.16 (m, 8H; CH(CH_2)R), 4.93 (br s, 4H; CHAr$_2$), 7.05 (s, 4H; ArH), 7.57 (s, 4H; ArH), 7.98 ppm (s, 8H; PzH); MS (CI): m/z (%): 1129 (100) [M^+].

Trisquinoxaline-bridged resorcinarene 9: Resorcin[4]arene **10** (1.63 g, 3 mmol), 2,3-dichloroquinoxaline (1.81 g, 9 mmol), and K$_2$CO$_3$ (1.24 g, 9 mmol) in dry Me$_2$SO (350 mL) were stirred at room temperature for 2 d. The reaction was quenched by the addition of HCl$_{aq}$ (10%), and the solid formed was filtered, washed with water, and dried. The crude product was purified by column chromatography on silica gel by using CH$_2$Cl$_2$/EtOAc (9:1 v/v) as eluent to give compound **9** as a white solid (0.53 g, 0.57 mmol, 19%). M.p. > 360 °C; ^{1}H NMR (300 MHz, CDCl$_3$): $\delta = 1.73$ (d, $^{3}J = 7.2$ Hz, 3H; CH_3), 1.79 (d, $^{3}J = 7.4$ Hz, 6H; CH_3), 1.83 (d, $^{3}J = 7.4$ Hz, 3H; CH_3), 4.53 (q, $^{3}J = 7.2$ Hz, 1H; CHAr$_2$), 5.54 (m, 3H; CHAr$_2$), 7.06 (s, 2H; ArH), 7.21 (s, 2H; ArH), 7.35 (s, 2H; ArH), 7.51 (m, 4H, AA' part of a AA'BB' system in QxH, Qx'H), 7.57 (dt, $^{3}J = 7.1$ Hz, $^{4}J = 1.1$ Hz, 2H; Qx'H), 7.73 (dd, $^{3}J = 7.1$ Hz, $^{4}J = 1.1$ Hz, 2H; Qx'H), 7.82 (m, 2H; BB' part of a AA''BB' system in QxH), 7.93 (dd, $^{3}J = 7.1$ Hz, $^{4}J = 1.1$ Hz, 2H; Qx'H), 8.09 (br s, 2H; ArOH), 8.11 ppm (s, 2H; ArH); MS (CI): m/z (%): 923 (100) [M^-].

Trisquinoxalinemethylene-bridged cavitand 3: A solution of CH$_2$BrCl (69 μL, 1 mmol) and trisquinoxaline-bridged resorcinarene **9** (0.23 g, 0.25 mmol) in dry Me$_2$SO (30 mL) were slowly added to a mixture of K$_2$CO$_3$ (0.12 g, 0.3 mmol) in dry Me$_2$SO (20 mL). The mixture was stirred at 50 °C for 12 h, then it was quenched by the addition of HCl$_{aq}$ (10%), and the solid formed was filtered, washed with water, and dried. The crude product was purified by column chromatography on silica gel by using CH$_2$Cl$_2$/EtOAc (97:3 v/v) as eluent to give compound **3** as a white solid (0.05 g, 0.05 mmol, 20%). M.p. > 360 °C; ^{1}H NMR (300 MHz, CDCl$_3$): $\delta = 1.78$ (d, $^{3}J = 7.4$ Hz, 3H; CH_3), 1.83 (d, $^{3}J = 7.5$ Hz, 6H; CH_3), 1.88 (d, $^{3}J = 7.5$ Hz, 3H; CH_3), 4.00 (d, $^{3}J = 7.2$ Hz, 1H; OCH$_{in}$O), 4.92 (q, $^{3}J = 7.4$ Hz, 1H; CHAr$_2$), 5.64 (d, $^{3}J = 7.2$ Hz, 1H; OCH$_{out}$O), 5.90 (m, 3H; CHAr$_2$), 7.20 (s, 2H; ArH), 7.33 (s, 2H; ArH), 7.34 (s, 2H; ArH), 7.48 (m, 4H; Qx'H), 7.56 (m, 2H, AA' part of a AA'BB' system in QxH), 7.68 (dd, $^{3}J = 8.1$ Hz, $^{4}J = 1.2$ Hz, 2H; Qx'H), 7.80 (m, 2H; BB' part of a AA'BB' system in QxH), 7.83 (dd, $^{3}J = 8.5$ Hz, $^{4}J = 1.5$ Hz, 2H; Qx'H), 8.26 ppm (s, 2H; ArH); MS (CI): m/z (%): 934 (100) [M^-].

Trisquinoxalinephosphonate-bridged cavitands 4 (in isomer) and 5 (out isomer): Phenylphosphonic dichloride (0.20 mL, 1.40 mmol) was slowly

added to a solution of trisquinoxaline-bridged resorcinarene **9** (0.26 g, 0.28 mmol) and Et₃N (0.39 mL, 2.80 mmol) in THF (100 mL). The solution was stirred at room temperature for 15 h, filtered, and the filtrate concentrated under vacuum. The crude product was purified by column chromatography on silica gel by using CH_2Cl_2/Me_2CO (19:1 v/v) as eluent to give compounds **4** (0.092 g, 0.09 mmol, 31%) and **5** (0.062 g, 0.06 mmol, 21%).

Data for 4: M.p. > 360°C; ^1H NMR (400 MHz, CDCl₃): $\delta = 1.84$ (m, 6H; CH_3), 1.88 (d, $^3J = 7.5$ Hz, 6H; CH_3), 4.87 (dq, $^3J = 7.5$ Hz, ^5J(H,P) = 2.2 Hz, 1H; $CHAr_2$), 5.97 (m, 3H; $CHAr_2$), 7.30 (m, 2H; AA′ part of a AA′BB′ system in Qx*H*), 7.32 (s, 2H; Ar*H*), 7.38 (s, 2H; Ar*H*), 7.39 (s, 2H; Ar*H*), 7.48 (m, 2H; Qx′*H*), 7.55–7.67 (m, 7H; BB′ part of a AA′BB′ system in Qx*H*, Qx′*H*, Ph*H*ₘ and Ph*H*ₚ), 7.74 (d, $^3J = 8.3$ Hz, 2H; Qx′*H*), 7.99 (ddd, ^3J(H,P) = 14.5 Hz, $^3J = 8.0$ Hz, $^4J = 1.5$ Hz, 2H; Ph*H*ₒ), 8.05 (d, $^3J = 8.3$ Hz, 2H; Qx′*H*), 8.35 ppm (s, 2H; Ar*H*); ^{31}P NMR (162 MHz, CDCl₃): $\delta = 9.85$ ppm (t, ^3J(H,P) = 14 Hz); FT-IR: $\tilde{\nu} = 1267$ cm^{-1} (P=O); MS (CI): m/z (%): 1044 (100) [M⁻].

Data for 5: M.p. > 360°C; ^1H NMR (400 MHz, CDCl₃): $\delta = 1.74$ (m, 9H; CH_3), 1.85 (d, $^3J = 6.9$ Hz, 3H; CH_3), 4.91 (q, $^3J = 7.0$ Hz, 2H; $CHAr_2$), 5.17 (q, $^3J = 6.9$ Hz, 1H; $CHAr_2$), 5.34 (q, $^3J = 7.3$ Hz, 1H; $CHAr_2$), 7.01 (s, 2H; Ar*H*), 7.10 (s, 2H; Ar*H*), 7.20 (s, 2H; Ar*H*), 7.38 (m, 2H; Ph*H*ₘ), 7.54–7.74 (m, 9H; AA′ part of a AA′BB′ system in Qx*H*, Qx′*H*, Ph*H*ₒ and Ph*H*ₚ), 7.77 (dd, $^3J = 8.0$ Hz, $^4J = 1.4$ Hz, 2H; Qx′*H*), 7.83 (s, 2H; Ar*H*), 7.89 (m, 2H; BB′ part of a AA′BB′ system in Qx*H*), 7.97 ppm (dd, $^3J = 8.2$ Hz, $^4J = 1.2$ Hz, 2H; Qx′*H*); ^{31}P NMR (162 MHz, CDCl₃): $\delta = 11.7$ ppm (t, ^3J(H,P) = 14 Hz); FT-IR: $\tilde{\nu} = 1264$ cm^{-1} (P=O); MS (CI): m/z (%): 1044 (100) [M⁻].

Trisquinoxalinephosphate-bridged cavitands 6 (in isomer) and 7 (out isomer): A solution of *p*-tolyl dichlorophosphate (84 μL, 0.50 mmol) in dry Me_2CO (10 mL) was slowly added to a solution of trisquinoxaline-bridged resorcinarene **9** (0.09 g, 0.10 mmol) and Et₃N (0.14 mL, 1 mmol) in dry Me_2CO (20 mL). The solution was stirred at room temperature for 12 h, filtered, and the filtrate concentrated under vacuum. The crude product was purified by column chromatography on silica gel by using hexane/EtOAc (1:1 v/v) as eluent to give compounds **6** (0.021 g, 0.02 mmol, 20%) and **7** (0.010 g, 0.01 mmol, 9%).

Data for 6: M.p. > 360°C; ^1H NMR (300 MHz, CDCl₃): $\delta = 1.79$ (d, $^3J = 5.5$ Hz, 3H; CH_3), 1.83 (d, $^3J = 6.3$ Hz, 3H; CH_3), 1.86 (d, $^3J = 5.7$ Hz, 6H; CH_3), 2.37 (s, 3H; CH_3-Ph), 4.71 (q, $^3J = 5.5$ Hz, ^5J(H,P) = 1.7 Hz, 1H; $CHAr_2$), 5.94 (m, 3H; $CHAr_2$), 7.21 (br s, 4H; Ph*H*), 7.30 (s, 2H; Ar*H*), 7.32 (m, 2H, AA′ part of a AA′BB′ system in Qx*H*), 7.35 (s, 2H; Ar*H*), 7.39 (d, ^4J(H,P) = 0.7 Hz, 2H; Ar*H*), 7.50 (m, 2H; Qx′*H*), 7.62 (m, 2H; Qx′*H*), 7.66 (m, 2H; BB′ part of a AA′BB′ system in Qx*H*), 7.75 (d, $^3J = 8.3$ Hz, 2H; Qx′*H*), 8.04 (d, $^3J = 8.3$ Hz, 2H; Qx′*H*), 8.33 ppm (s, 2H; Ar*H*); ^{31}P NMR (81 MHz, CDCl₃): $\delta = -18.7$ ppm (s); FT-IR: $\tilde{\nu} = 1336$ cm^{-1} (P=O); MS (CI): m/z (%): 1075 (100) [M⁻].

Data for 7: M.p. > 360°C; ^1H NMR (300 MHz, CDCl₃): $\delta = 1.84$ (d, $^3J = 5.6$ Hz, 6H; CH_3), 1.87 (d, $^3J = 5.4$ Hz, 3H; CH_3), 1.88 (d, $^3J = 5.2$ Hz, 3H; CH_3), 2.20 (s, 3H; CH_3-Ph), 4.94 (q, $^3J = 5.4$ Hz, ^5J(H,P) = 1.9 Hz, 1H; $CHAr_2$), 5.86 (m, 3H; $CHAr_2$), 6.60 (d, $^3J = 8.2$ Hz, 2H; Ph*H*), 6.81 (d, $^3J = 8.2$ Hz, 2H; Ph*H*), 7.36 (s, 2H; Ar*H*), 7.39 (s, 2H; Ar*H*), 7.45 (d, ^4J-(H,P) = 1.0 Hz, 2H; Ar*H*), 7.47–7.55 (m, 8H; AA′ part of a AA′BB′ system in Qx*H*, Qx′*H*), 7.80 (m, 2H; BB′ part of a AA′BB′ system in Qx*H*), 7.84 (d, $^3J = 6.1$ Hz, 2H; Qx′*H*), 8.16 ppm (s, 2H; Ar*H*); ^{31}P NMR (81 MHz, CDCl₃): $\delta = -24.0$ ppm (s); FT-IR: $\tilde{\nu} = 1333$ cm^{-1} (P=O); MS (CI): m/z (%): 1075 (100) [M⁻].

Determination of thermodynamic and kinetic parameters for conformational switching and solvent scan by NMR spectroscopy: ^1H and ^{13}C NMR spectra were recorded with a Varian Mercury 300 spectrometer. Deuterated solvents were used as internal references. For the variable temperature experiments, the temperature was calibrated with 100% MeOH ($T \leq 313$ K) or CH_2OH–CH_2OH ($T \geq 313$ K) reference samples. Temperature regulation was stable within ±0.5° between 363 K and 243 K, and within ±1.5° at lower temperatures. Fitting of NMR spectra was performed with the gNMR v3.6 for Macintosh program (Cherwell Scientific, Oxford, UK). For the lineshape fitting of the kite 1–kite 2 equilibrium of the cavitand **2**, all the aromatic protons and methine proton were included into a two-site exchange model.

Determination of activation enthalpy and entropy was based on Equation (1)[15] in which k [Hz] is an exchange constant obtained from spectral fitting, T the temperature in Kelvin and $a = 4.575 \times 10^{-3}$ for $\Delta H^{\pm}$ in kcal mol^{-1} and $\Delta S^{\pm}$ in kcal mol^{-1} K^{-1}.

$$\log(k/T) = -\Delta H^{\pm}/aT + \Delta S^{\pm}/a + 10.319 \tag{1}$$

According to Equation (1), a plot of $\log(k/T)$ versus $1/T$ (Eyring plot) has a slope of $(-\Delta H^{\pm}/a)$ and an intercept at $1/T = 0$ of $(\Delta S^{\pm}/a + 10.319)$. Equation (2) was used to calculate the free energy of activation at the temperature of coalescence[16] of an equally populated two-site systems.

$$\Delta G_c^{\pm} = aT[9.972 + \log(T/\delta\nu)] \tag{2}$$

In Equation (2) T is the temperature in Kelvin, $\delta\nu$ [Hz] the chemical shift between two coalescing resonances in the absence of exchange, and $a = 4.575 \times 10^{-3}$ for $\Delta G_c^{\pm}$ in kcal mol^{-1}.

X-ray crystallographic studies. The crystal structure of solvates **2**, **3**, and **4** were determined by single-crystal X-ray diffraction methods. Crystallographic and experimental details for the structures are summarized in the Supporting Information (Table 1SI). Crystals of **2** suitable for X-ray analysis were obtained exposing a solution of the compound in dichloromethane to ethanol vapors; as a consequence, each cavitand crystallized with three alcohol molecules in the asymmetric unit. Due to statistical disorder, it was not possible to univocally assign the oxygen atoms of the ethanol molecules, which were therefore considered as carbon atoms during the refinement of the structure.

Intensity data and cell parameters were recorded on a Siemens AED (**3** and **4**) and on an Enraf Nonius CAD4 (**2**) diffractometer using graphite-monochromated Cu$_{Ka}$ radiation. One standard reflection, collected every 100 to monitor crystal decay and instrumental linearity, showed a linear decay of almost 20% for compound **2**. The intensities were corrected for Lorentz and polarization but not for absorption.

The structures were solved by Direct Methods using the SIR92 program[17] and refined by full-matrix least-squares procedures (based on F_c^2 for **2** and **4** and on F_o for **3**), using the SHELXL-97 program.[18] In compound **4**, all the atoms were refined isotropically, while in **2** and **3** all non-hydrogen atoms were refined with anisotropic atomic displacements (with the exception of the atoms of the ethyl acetate molecule inside the cavity in **3**, the three ethanol molecules and the terminal carbon atoms of three aliphatic chains in **2**, all were affected by statistic disorder). The hydrogen atoms were introduced into the geometrically calculated positions and refined "riding" on the corresponding parent atoms for all the compounds. The weighting scheme used in the last cycle of refinement was $w = 1/[\sigma^2 F_o^2 + (0.1115 P)^2]$ for **2**, $w = 1/[\sigma^2 F_o^2 + (0.1821 P)^2 + 21.8601 P]$ for **3**, and $w = 1/[\sigma^2 F_o^2 + (0.1600 P)^2 + 20.4294 P]$ for **4**, in which $P = (F_o^2 + 2F_c^2)/3$. Molecular geometry calculations were carried out using the PARST97 program.[19] Drawings were obtained by ORTEP3 in the WinGX suite[20] and by DS ViewerPro.[21] All calculations were carried out on a DIGITAL Alpha Station 255 computer.

CCDC-285183–285185 contain the supplementary crystallographic data for this paper. These data can be obtained free of charge from The Cambridge Crystallographic Data Centre via www.ccdc.cam.ac.uk/data_request/cif.

[1] a) J. R. Moran, S. Karbach, D. J. Cram, *J. Am. Chem. Soc.* **1982**, *104*, 5826–5828; b) J. R. Moran, J. L. Ericson, E. Dalcanale, J. A. Bryant, C. B. Knobler, D. J. Cram, *J. Am. Chem. Soc.* **1991**, *113*, 5707–5714; c) D. J. Cram, H.-J. Choi, J. A. Bryant, C. B. Knobler, *J. Am. Chem. Soc.* **1992**, *114*, 7748–7765; d) D. J. Cram, J. M. Cram, *Container Molecules and Their Guests*, Royal Society of Chemistry, Cambridge, **1994**, pp. 107–130.

[2] F. Hof, S. L. Craig, C. Nuckolls, J. Rebek, Jr., *Angew. Chem.* **2002**, *114*, 1556–1578; *Angew. Chem. Int. Ed.* **2002**, *41*, 1488–1508.

[3] a) E. Dalcanale, P. Soncini, G. Bacchilega, F. Ugozzoli, *J. Chem. Soc. Chem. Commun.* **1989**, 500–502; b) P. Soncini, S. Bonsignore, E. Dalcanale, F. Ugozzoli, *J. Org. Chem.* **1992**, *57*, 4608–4612; c) T. Heinz, D. M. Rudkevich, J. Rebek Jr., *Nature* **1998**, *394*, 764–765; d) T. Heinz, D. M. Rudkevich, J. Rebek, Jr., *Angew. Chem.* **1999**, *111*, 1206–1209; *Angew. Chem. Int. Ed.* **1999**, *38*, 1136–1139; e) S. K. Körner, F. C. Tucci, D. M. Rudkevich, T. Heinz, J. Rebek, Jr., *Chem. Eur. J.* **2000**, *6*, 187–195; f) F. Hof, J. Rebek, Jr., *Proc. Natl. Acad. Sci. USA* **2002**, *99*, 4775–4777.

[4] H. Ihm, J.-S. Ahn, M. S. Lah, Y. H. Ko, K. Paek, *Org. Lett.* **2004**, *6*, 3893–3896.

[5] a) P. J. Skinner, A. G. Cheetham, A. Beeby, V. Gramlich, F. Diederich, *Helv. Chim. Acta* **2001**, *84*, 2146–2153; b) V. A. Azov, B. Jaun, F. Diederich, *Helv. Chim. Acta* **2004**, *87*, 449–462.

[6] a) P. Amrhein, A. Shivanyuk, D. W. Johnson, J. Rebek Jr., *J. Am. Chem. Soc.* **2002**, *124*, 10349–10358; b) M. Frei, F. Marotti, F. Diederich, *Chem. Commun.* **2004**, 1362–1363.

[7] a) Special issue on molecular machines: *Acc. Chem. Res.* **2001**, *34*, 410–522; b) *Molecular Switches* (Ed.: B. L. Feringa), Wiley-VCH, Weinheim, **2001**.

[8] a) Y. Yamakoshi, R. R. Schlittler, J. K. Gimzewski, F. Diederich, *J. Mater. Chem.* **2001**, *11*, 2895–2897; b) V. A. Azov, F. Diederich, Y. Lill, B. Hecht, *Helv. Chim. Acta* **2003**, *86*, 2149–2155; c) V. A. Azov, P. J. Skinner, Y. Yamakoshi, P. Seiler, V. Gramlich, F. Diederich, *Helv. Chim. Acta* **2003**, *86*, 3648–3670.

[9] V. A. Azov, A. Schlegel, F. Diederich, *Angew. Chem.* **2005**, *117*, 4711–4715; *Angew. Chem. Int. Ed.* **2005**, *44*, 4635–4638.

[10] a) T. Lippmann, H. Wilde, E. Dalcanale, L. Mavilla, G. Mann, U Heyer, S. Spera, *J. Org. Chem.* **1995**, *60*, 235–242; b) P. Jacopozzi, E. Dalcanale, S. Spera, L. A. J. Chrisstoffels, D. N. Reinhoudt, T. Lippmann, G. Mann, *J. Chem. Soc. Perkin Trans. 2* **1998**, *3*, 671–678.

[11] M. Vincenti, E. Dalcanale, *J. Chem. Soc. Perkin Trans. 2* **1995**, *6*, 1069–1076.

[12] a) M. H. Abraham, *Chem. Soc. Rev.* **1993**, *22*, 73–83; b) S. D. Martin, C. F. Poole, M. H. Abraham, *J. Chromatogr.* **1998**, *805*, 217–235; c) Y. Ishihama, N. Asakawa, *J. Pharm. Sci.* **1999**, *88*, 1305–1312.

[13] L. Abis, E. Dalcanale, A. Du Vosel, S. Spera, *J. Org. Chem.* **1988**, *53*, 5475–5479.

[14] J. Adachi, N. Sato, *J. Org. Chem.* **1972**, *37*, 221–225.

[15] J. Sandström, *Dynamic NMR Spectroscopy*, Academic Press, London, **1982**, pp. 93–123.

[16] Free activation energies at the temperatures of coalescence ($\Delta G_c^{\pm}$) were determined to compare their values with the calculated ones by using the $\Delta H^{\pm}$ and $\Delta S^{\pm}$ values obtained from the Eyring plot. For all coalescence temperatures of different exchanging protons the deviation was less than ± 0.3 kcal mol^{-1}.

[17] A. Altomare, G. Cascarano, C. Giacovazzo, A. Gualiardi, M. C. Burla, G. Polidori, M. Camalli, *J. Appl. Crystallogr.* **1994**, *27*, 435–436.

[18] G. M. Sheldrick, SHELX-97, University of Göttingen, Göttingen (Germany), **1997**.

[19] M. Nardelli, PARST97, updated version of PARST95, *J. Appl. Crystallogr.* **1995**, *28*, 659.

[20] Ortep3 in the WinGX suite, L. J. Farrugia, *J. Appl. Crystallogr.* **1997**, *30*, 565.

[21] DS ViewerPro 5.0, Accelerys Inc., **2002**.